

CHEMNANOMAT

CHEMISTRY OF NANOMATERIALS FOR ENERGY, BIOLOGY AND MORE

www.chemnanomat.org

Accepted Article

Title: Tracking the dimensionality transition from a three dimensional single crystal to a two dimensional perovskite

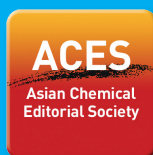
Authors: Idan Cohen, Małgorzata Wierzbowska, Ben Aizenshtein, and Lioz Etgar

This manuscript has been accepted after peer review and appears as an Accepted Article online prior to editing, proofing, and formal publication of the final Version of Record (VoR). The VoR will be published online in Early View as soon as possible and may be different to this Accepted Article as a result of editing. Readers should obtain the VoR from the journal website shown below when it is published to ensure accuracy of information. The authors are responsible for the content of this Accepted Article.

To be cited as: *ChemNanoMat* 2024, e202300625

Link to VoR: <https://doi.org/10.1002/cnma.202300625>

A Journal of



WILEY-VCH

Tracking the dimensionality transition from a three dimensional single crystal to a two dimensional perovskite

Idan Cohen¹, Małgorzata Wierzbowska², Ben Aizenshtein¹, and Lioz Etgar^{1,*}

¹The Hebrew University of Jerusalem, Institute of Chemistry, Casali Center for Applied Chemistry, Jerusalem, 91904, Israel

²Institute of High Pressure Physics Polish Academy of Sciences, Sokołowska 29/37, 01-142 Warsaw, Poland

E-mail address: lioz.etgar@mail.huji.ac.il

Abstract

This work carefully studied the transition from 3D perovskite to 2D perovskite. Our system includes single crystals (SCs) of MAPbBr₃, which were dipped in a solution of barrier molecules. Three monoammonium cations and one di-ammonium cation were studied. Absorbance and cathodoluminescence were used to follow the formation of low-dimensional perovskite on the SC surface. Quantitative nuclear magnetic resonance and scanning electron microscopy assist in quantitatively tracking the exchange process. We followed the barrier molecules' concentration during the exchange process and their penetration depth into the 3D single crystal. The short aliphatic chain penetrates much farther into the crystal (ca. 450 μm) than the long aliphatic chain barrier molecule. In contrast, the process time is the opposite: the long aliphatic chain requires 5 days to achieve an equilibrium state compared with 15 days for the short aliphatic chain. *Ab initio* calculations indicate that the exchange process initiates due to the methylammonium vacancies on the surface, and the process is inhibited by the interactions between the -NH₃ group and the PbBr₂ planes. This work sheds light on the kinetics and thermodynamics of the transition from 3D to 2D perovskites, which is important for stabilizing the hybrid perovskites.

Keywords: Single Crystal; 2D perovskite; barrier molecules; Q-NMR

Introduction

Lead halide perovskite has gained attention due to its special properties, such as a high absorption coefficient, long diffusion length, tunable and direct band gap, preparation simplicity, and cost-effectiveness. These unique properties make perovskite a promising material for use in optoelectronic devices [1–3]. The perovskite structure is based on the formula ABX_3 , where A is either an organic or inorganic monovalent cation ($CH_3NH_3 = MA$, $CH(NH_2)_2 = FA$ and Cs), B is a divalent metallic cation (B = Pb and Sn), and X is a halide anion (X = Cl, Br, and I). The 3D structure of the perovskite is based on octahedrons having a BX_6 formula connected to each other, whereas in the cage, which formed between the octahedrons, a small A cation is positioned. A special feature of this structure is that it can contain a mixture of ions and cations [4,5]. One way to form multi-ion perovskite materials in optoelectronic devices is through ion exchange reactions. These reactions have been extensively studied in recent years on different systems such as perovskite nanocrystals, thin films, and single crystals (SCs) [6–10]. When the A cation is larger than the cage between the octahedrons, it separates the BX_6 octahedrons, resulting in two-dimensional (2D) perovskite [11,12] according to the chemical formula $(R-NH_3)A_{n-1}B_nX_{3n+1}$, where R is a large aliphatic group and n is the number of octahedron rows between the large cations. Recently several reports have indicated that the formation of a 2D perovskite monolayer on top of 3D perovskite can assist in stabilizing the 3D perovskite while still maintaining high photovoltaic (PV) performance [11–14].

Giles E. Eperon et al. reported that cation exchange of methylammonium lead iodide ($MAPbI_3$) and formamidinium lead iodide ($FAPbI_3$) thin films dipped inside FAI and MAI solutions improve the PV performance of the perovskite solar cells (PSCs) [15]. On the other hand, Nathan T. Shewmon et al. showed that when methylammonium lead bromide ($MAPbBr_3$) SC and thin films were dipped inside $MAPbI_3$ solution, the formation of an $MAPbI_3$ layer on the SC was formed predominantly by an anion exchange reaction [9]. Moreover, they showed that Cs cation treatment of 2D perovskite SC induced a transition from 2D to 3D by a cation exchange mechanism [9]. In addition, Y. Zhang et al. monitored the kinetics of the cation exchange process on cesium lead bromide ($CsPbBr_3$) nanoplates with BuAI by using microscopic photoluminescence imaging, recognizing the transition dimensionality during the anion exchange [10].

This work focuses on the molecular transition from 3D perovskite to 2D perovskite in single crystals. Qualitative and quantitative monitoring of the dimensional transition was done in macro scales of perovskite shading more light on this process. Butylammonium Bromide (BuABr), Hexylammonium Bromide (HeABr), Octylammonium Bromide (OcABr), and 1,4 – Butylenediammonium Bromide (BuDABr₂) were used as the long organic cations (barrier molecules) in this study. 2D perovskite has several structures based on the barrier molecule being used. Ruddlesden-Popper (RP) structure having the formula (R-NH₃)₂A_{n-1}B_nX_{3n+1} is formed when mono ammonium barrier molecules are used[16,17] while Dion-Jacobson (DJ) structure is formed when diammonium barriers are being used having the formula ((NH₃)-R-(NH₃))A_{n-1}B_nX_{3n+1}. [18,19]

In this work BuABr, HeABr and OcABr are forming 2D perovskite with RP structure and BuDABr₂ is forming 2D perovskite with DJ structure.

In order to quantitatively monitor this process, MAPbBr₃ SCs were dipped into solutions that contained different barrier molecules. Quantitative nuclear magnetic resonance (Q-NMR), scanning electron microscopy (SEM), and absorbance measurement were used to follow the 3D to 2D transition process over time. Single-crystal X-ray diffraction (S-XRD) assists in finding the exact structure that formed. In addition, cathodoluminescence (CL) was used to optically detect different dimensionalities over a single crystal.

Results and discussion

In order to investigate the transition from 3D perovskite to 2D perovskite, MAPbBr₃ SC was dipped into different solutions of barrier molecules and the transition was tracked over time. Three monoammonium linear barriers were studied: BuABr, HeABr, and OcABr (see Fig. 1a-c). Figures 1d-f show photographs of the SCs that were cut in the middle after being dipped in the corresponding barrier molecules for 30 days. It can be seen that the middle of the SC has an orange color, which indicates MAPbBr₃ perovskite, whereas the surface has a different color, which suggests a different perovskite dimensionality, as discussed below. After BuABr treatment, the color becomes yellow (Fig. 1d), compared with HeABr and OcABr treatments, after which the color becomes white (Fig. 1e and f).

The corresponding SCs were taken for SEM analysis, as shown in Figures 1g-i. The difference between the surface and the bulk is clear. The morphology of the bulk is more uniform than the morphology of the surface, which suggests that the surface reacted with the barrier molecule in the dipping solution.

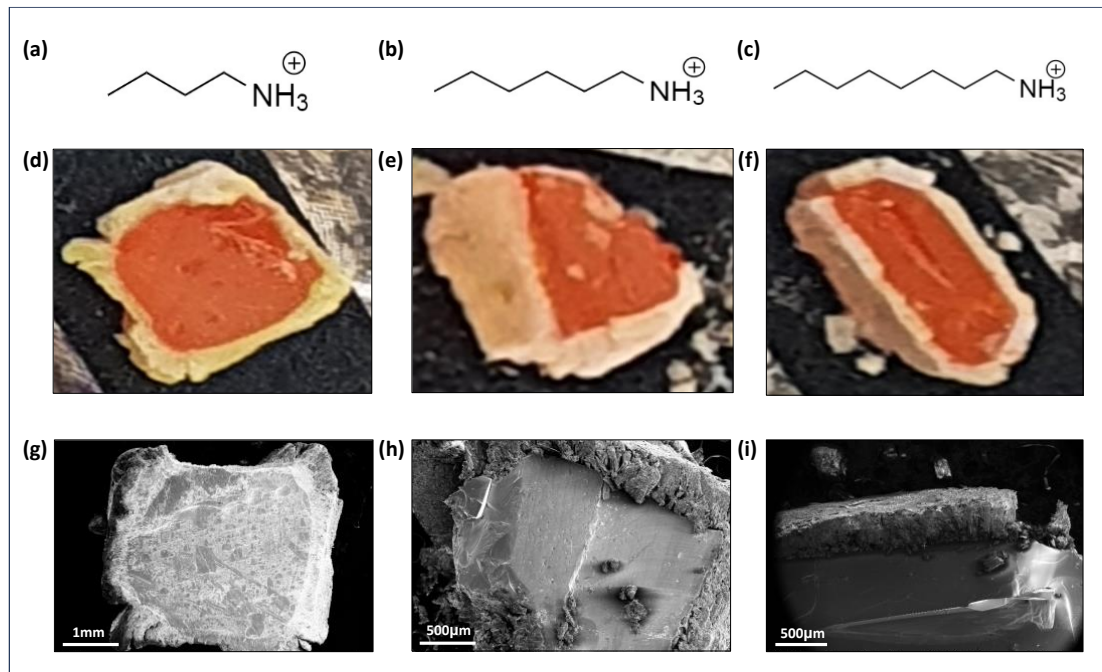


Figure 1. The structure of (a) the BuABr molecule. (b) the HeABr molecule. (c) the OcABr molecule. (d) Photograph of SC after 30 days of treatment in BuABr solution. (e) After 30 days of treatment in HeABr. (f) After 30 days of treatment in OcABr. (g) The corresponding SEM image of BuABr. (h) The corresponding SEM image of HeABr. (i) The corresponding SEM image of OcABr.

Single-crystal X-ray diffraction (s-XRD) was measured in order to analyze the material phases that were formed on the SC surface. The s-XRD decoding for 3D SC that was dipped in a BuABr solution for 40 days is presented in Figure S1 in the supporting information (SI). The decoding is separated from the bulk of the SC and from the surface of the SC, which shows that the bulk is 3D perovskite, whereas the surface formed 2D perovskite having the RP structure. In the case of BuDABr₂, it was also found that the surface is forming 2D perovskite similar to the BuABr case but since it is a diammonium barrier molecule DJ structure was formed (Figure S2).

pXRD confirms the formation of 2D perovskite in the case of HeABr and OcABr as the barrier molecules. The pXRD pattern can be observed in figure S3 which shows XRD peaks at small angles confirming the formation of low dimensional perovskite. [20]

Next, the transition from 3D to 2D over time was tracked for different monoammonium barrier molecules. Figures 2a-c show the absorbance spectra for the monoammonium barriers at different times. In all the barrier molecules, the absorbance onset did not change (at 581nm). However, looking at shorter wavelengths of BuABr (Figure 2a), starting from 10 days to 30 days, more features in the absorbance spectra began to appear. These features are due to the quantization effect, more transitions are pronounced at shorter wavelengths in the case of low dimensional perovskite, therefore the absorbance spectra can indicate on the dimensionality that formed over time during the dipping.

Regarding the HeABr and OcABr treatments, new features start to appear over time at short wavelengths but there are fewer regarding BuABr (Figures 2b, c). This might be due to the length of the barrier molecule, which plays a role in the kinetics of the transition from 3D to 2D perovskite in the SC. In order to observe more information on the additional features at the short wavelength in the absorbance spectra, thin films of 2D perovskite at various n values were synthesized (figure S4). A red shift was observed between the absorbance of the single crystal and the thin films. This red shift is due to the SC thickness vs. the thin films as was reported earlier.[20] Moreover it can be seen that these features at high energy are systematically red shifted which support our conclusion that dimensionality was formed.

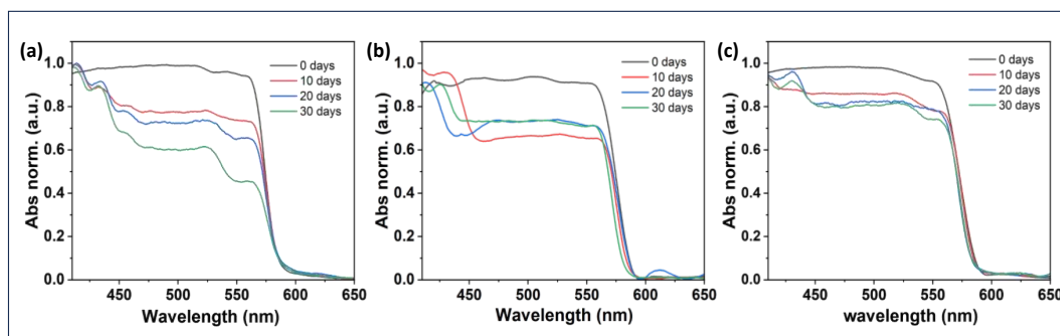


Figure 2. Single-crystal absorbance at different dipping times in the barrier solution. (a) Dipping in BuABr solution. (b) Dipping in HeABr solution. (c) Dipping in OcABr solution.

For longer barrier molecules, the transition is slower and it is more difficult to occur, which will be discussed in more detail. Moreover, it can be seen that although the new features at short wavelengths start to appear with time, the intensity of the onset of the

3D decreases over time. This observation indicates the formation of new 2D perovskite populations over the 3D perovskite.

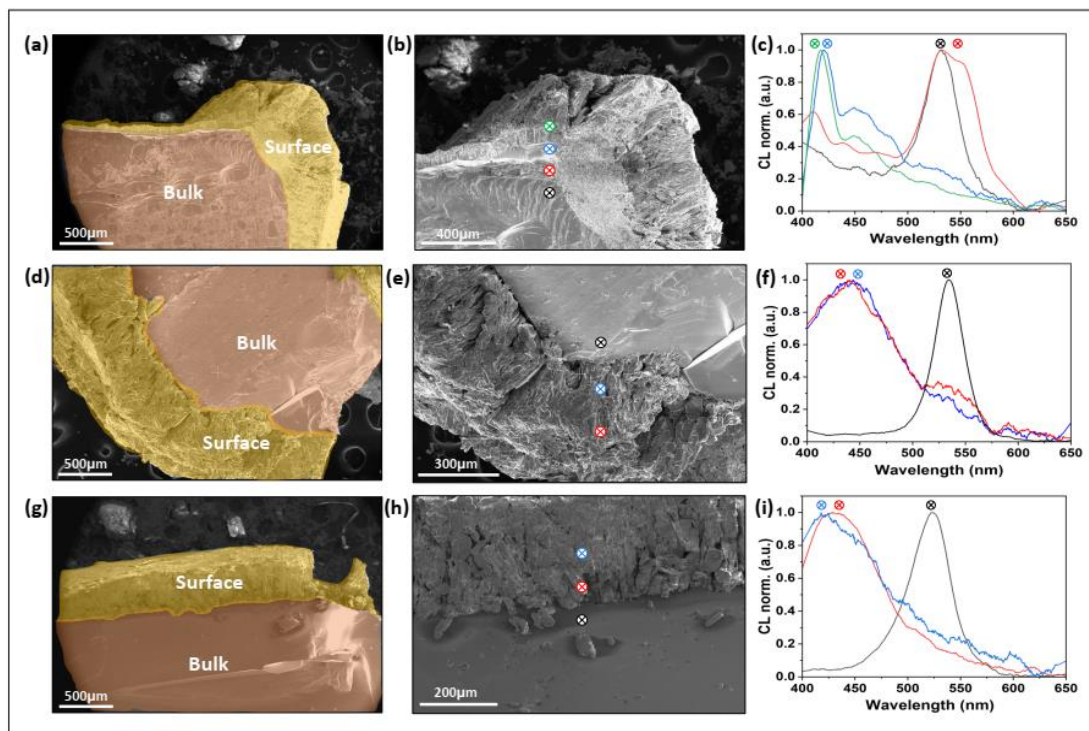


Figure 3. Cathodoluminescence (CL) measurements. (a) SC after 30 days of BuABr treatment. (b) Zoom in on a and the corresponding measurement points. (c) CL peaks of the points mentioned in b. (d) SC after 30 days of HeABr treatment. (e) Zoom in on d and the corresponding measurement points. (f) CL peaks of the points mentioned in e. (g) SC after 30 days of OcABr treatment. (h) Zoom in on g and the corresponding measurement points. (i) CL peaks of the points mentioned in h.

In addition to the absorbance measurements over time, cathodoluminescence (CL) was used to locally detect the optical properties of the SC following its transition from 3D to 2D. CL measurements are performed inside high-resolution SEM, which allows observing luminescence spectra at a very high resolution from a specific area in the sample. Therefore this measurement can provide the existence of various n values at the SC's surface. Figures 3a, b, d, e, g, and h show a cross-section SEM of the SCs after 30 days of treatment in the solution of barrier molecules.

The CL measurements were taken from the bulk area toward the surface of the SC. The black point was taken from the bulk in all three cases; the corresponding CL peaks can

be seen in Figures 3c, f, and I. In all cases, the CL peak from the bulk appears at 539 nm, which agrees well with 3D MAPbBr₃ SC.

The difference between the onset in the absorbance spectra and the CL peak is due to the SC thickness. The absorbance measurement is taken from the bulk of the sample, whereas the CL is taken in HR-SEM from a specific location on the surface of the sample. Consequently, the emission is reabsorbed by the SC, which is responsible for the large shift of the emission spectra. It was reported that a spectral shift in the emission between the surface and bulk can reach ~10 meV in SCs [21].

Except for the black point peak, which was taken from the bulk of the SC and appears in each of the barrier molecules, the red, blue, and green peaks were taken from the SC surface. (The red point is closer to the bulk area, whereas the blue point is farther away from the bulk.) The CL of these points is blue-shifted compared to the bulk peak (the black point), which clearly indicates that low-dimensional perovskite was formed on the SC surface. The specific position changes slightly, depending on the barrier molecule. Moreover, as can be seen, the red, blue, and green peaks have a tail toward longer wavelengths (overlapping the black peak), which indicates that some 3D structure still exists on the SC surface. It can be concluded that the SC surface transitions to low-dimensional perovskite probably with different *n* values including some 3D residues. Additional support regarding this observation is provided by the s-XRD, as presented in Figure 1S. The measurement was done on a specific area at the bulk and on a specific area on the surface. The bulk measurement shows 3D perovskite, whereas the surface shows a 2D structure with *n*=1.

In order to provide quantitative information on the transition from 3D to 2D perovskite in the SC, Quantitative Nuclear magnetic resonance (Q-NMR) was performed. In this experiment, the solution of the barrier molecule was taken for Q-NMR measurements following various dipping times. Our hypothesis is that the change in the barrier molecule concentration and the methyl ammonium concentration in the dipping solution would provide an indication of the kinetic exchange process.

At the beginning of the experiments, only the barrier molecule can be recognized; however, over time, new additional peaks start to appear that are associated with the MA molecules, as shown in Figures 4a and b regarding BuABr. (Figures S5 and S6 show the NMR spectra for the other barrier molecules HeABr and OcABr) The change in the concentration of the barrier molecules at different dipping times was studied, as shown in Figure 4c. The negative change in the barrier molecules' concentration over

time indicates the exchange process; more barrier molecules are consumed from the dipping solution and intercalate into the SC. Finally, the concentration reached a minimum, as shown in Figures 4c and S7 for OcABr. It was found that the methylammonium peak appeared only when the barrier molecule is present inside the solution. Figure S8 shows Q-NMR spectra of MAPbBr₃ SC without the barrier molecule in the solution.

The Q-NMR measurements indicate that a difference exists in the kinetics between the barrier molecules: in a short aliphatic chain, the process is much faster than in a longer aliphatic chain. Figure 4d shows the change in the MA concentration in the dipping solution for different barrier molecules. The increase in the MA concentration is in agreement with the decrease in the concentration of the barrier molecules. The MA concentration increases faster for a short aliphatic chain.

The Q-NMR provides us with several conclusions as follows: (i) There is an exchange between the barrier molecule and the MA molecules coming from the SC. (ii) The kinetics differs for different barrier molecules: the shorter aliphatic chain exchanges the MA molecules faster inside the SC than does the longer aliphatic chain barrier molecule. (iii) Each barrier molecule has a different equilibrium state that is associated with different penetration depths of the barrier molecule into the SC (discussed next).

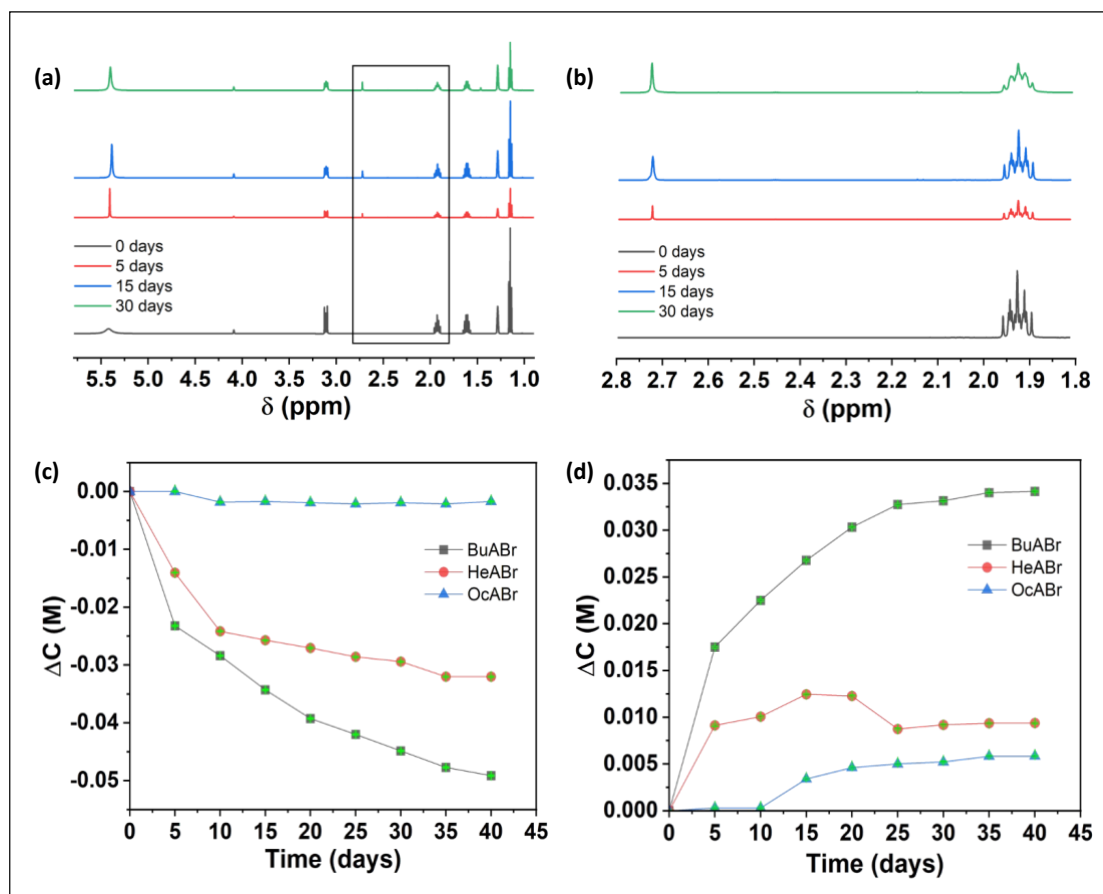


Figure 4. Q-NMR experiment and the resulting delta concentration (ΔC) data. (a) NMR spectra at different dipping times during the BuABr experiment. (b) Zoom in on the marked area that appears in a. (c) The barrier molecule concentration as a function of the dipping time calculated from the NMR. (d) The MA concentration as a function of the dipping time calculated from the NMR for different barrier molecules.

In order to further investigate the exchange process and to prove that a 2D structure formed on the SC surface, the penetration depth (PD) of the barrier molecule into the SC was measured. The SEM cross-section of SCs at different dipping times was characterized for the various barrier molecules. Figure 5a shows a SEM cross-section of the SC when BuABr is the barrier molecule. Figures S9-12 present the SEM cross-section of the other barrier molecules. The different parts can be observed in the cross-section SEM (Figure 5a), namely, the 2D perovskite on the SC surface and the 3D part at the bulk of the SC. This 2D perovskite's thickness was measured at various dipping times, as presented in the graph in Figure 5b. It can be seen that in a shorter aliphatic chain the penetration depth is larger than in the other barrier molecules with longer aliphatic chains. Moreover, in shorter barrier molecules there are more molecules that penetrate into the SC, in agreement with the Q-NMR results. As a result, more time is needed for this process to occur, since the extent of 2D perovskite formation is greater.

Regarding BuABr, the penetration depth is 450 μm , which takes approximately 15 days, whereas the penetration depth for OcABr is 150 μm , which occurred after 10 days.

All characterizations, i.e., Q-NMR, PD, and CL, indicate that a transfer occurs from 3D perovskite to 2D perovskite on the SC surface. The extent and the kinetics of the 2D formation depend on the type of barrier molecules. It is clear that the bulk of the SC remains 3D perovskite; however, the surface forms low-dimensional perovskite with mixed n values. Figure 5f shows a schematic illustration of the SC transition process.

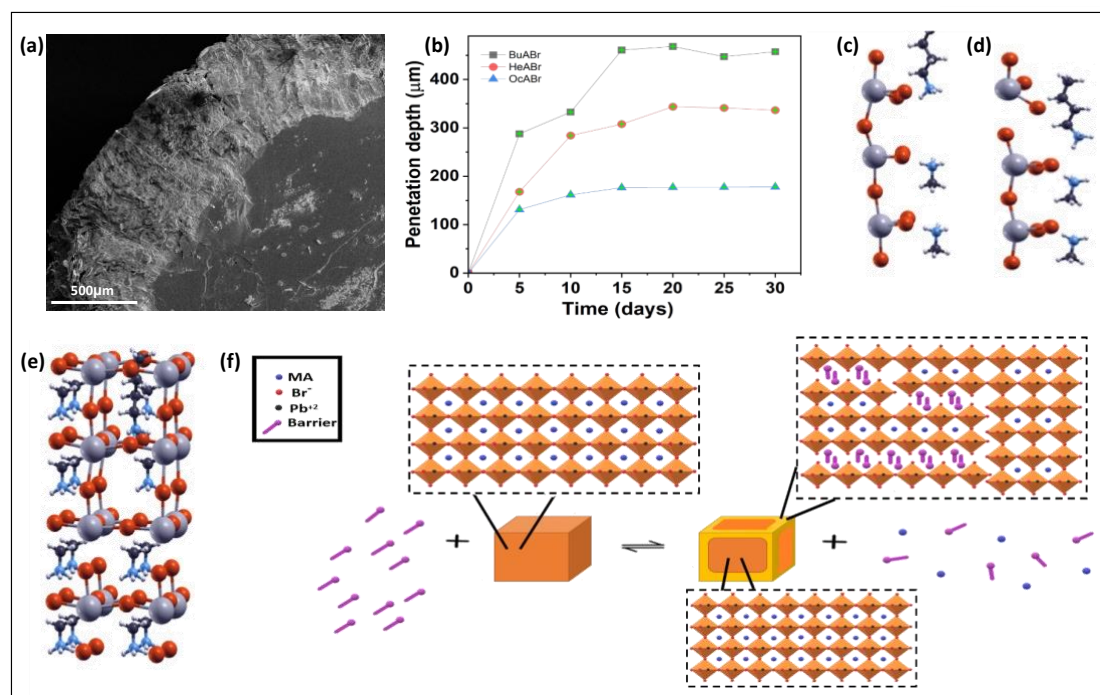


Figure 5. (a) Cross-section SEM pictures of the SC for BuABr after 25 days in the dipping solution. (b) Penetration depth (PD) as a function of time. (c-e) Free stages of the barrier penetration into the 3D crystal with MA vacancies; the plots of elementary cells. (f) Schematic illustration of the exchange process from 3D to 2D perovskite in SC.

In addition to the monoammonium barrier molecules, the di-ammonium barrier molecule, BuDABr₂, was also studied to elucidate its kinetic and dimensionality transition. MAPbBr₃ SC was dipped for 30 days in the BuDABr₂ barrier molecule solution. A photograph of the cut SC can be seen in Figure 6a and its corresponding absorbance can be seen in Figure 6b. Similar to the monoammonium barrier molecules, the absorbance onset did not shift over time. However, some features appeared in the absorbance at a shorter wavelength after 20 and 30 days. In comparison to BuABr and

the other barrier molecules, more time is needed for the 2D perovskite to be formed on the surface of the SC. When the SC is dipped in the BuDABr₂ solution for more than 30 days, some of the 2D perovskite starts to dissolve back into the barrier solution.

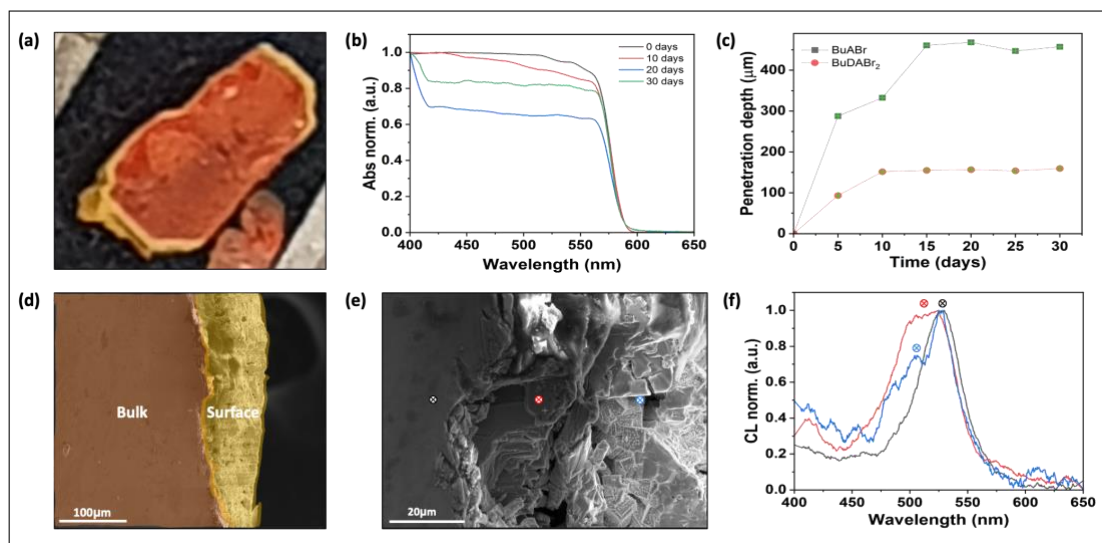


Figure 6. BuDABr₂ SC. (a) Photograph of the SC after 30 days of dipping. (b) SC absorbance at different dipping times. (c) Penetration depth at different times. (d) SEM picture after 30 days of treatment. (e) SEM image focusing on the CL measurement area. (f) Specific points CL spectra from the measurements were taken after 30 days of dipping.

The PD measurements (Figure 6c) showed that BuDABr₂ has a smaller penetration depth than does BuABr. BuDABr₂ penetrates 150 μm after 10 days into the SC and does not change anymore, whereas BuABr penetrates 450 μm after 15 days.

Figure 6d, e, and f show the SEM images and the corresponding CL measurements for the BuDABr₂ barrier molecules. Similar to the monoammonium barrier molecules, additional peaks associated with 2D perovskite can be observed; however, here the peaks are slightly shifted to blue, in contrast with the monoammonium barrier molecules.

Based on these characterizations, it can be concluded that the kinetics of 2D perovskite is slower for diammonium linear barrier molecules compared with the monoammonium linear barrier molecules.

The BuABr molecules are polar, whereas the BuDABr₂ molecules are nonpolar. The polar molecules' velocity is higher than that of the non-polar molecules in the solution. Molecules with higher velocity will have a higher probability to penetrate into the SC than molecules with lower velocity. These molecules, which have a high probability to

penetrate into the SC, will react better with the 3D perovskite and will transition to 2D perovskite. Additional reason is due to the difference in the 2D structure which formed by the BuABr and the BuDABr₂. The BuABr is forming RP structure which has larger distance between the layers than the DJ structure which formed by the BuDABr₂ barrier. Therefore the penetration depth of the diammonium barrier will be shorter than the monoammonium.

Density functional theory (DFT) calculations were performed to assist in explaining the observed ion exchange process. We assumed that some MA vacancies are present in the 3D perovskite crystal and that their distribution is higher on the surface than in the bulk. [22] Moreover, we considered contributions from two competitive phenomena.

The first effect is destructive for the crystal. When the density of the barrier molecules was set on the surface at 100%, it was found that all barrier molecules enter the 3D crystal only at the depth of the first PbBr₂ plane (the elementary cell can be seen in Figure 5c). When the NH₃⁺ group of barrier molecules was pushed deeper, it was found that the PbBr₂ crystal lattice locally breaks (Figure 5d). Furthermore, we observed that by enlarging the unit cell laterally by a factor of four and placing only 25% of the barrier molecules, the allowed penetration depth is deeper; the process stops at the second PbBr₂ plane (Figure 5e). This means that a small amount of barrier molecules can penetrate much deeper if the MA vacancies are still accessible.

The second effect is the opposite for the crystal. Local damage to the PbBr₂ crystal lattice near the barrier molecules is reconstructed, leading to a new crystal phase that is quasi-2D. The formation energies of such a phase (for the formula unit of the perovskite surface) bind more for long molecules with one NH₃ group (-2.17 eV for BuA, -2.90 eV for HeA, -2.65 eV for OcA) than for a short molecule with two NH₃⁺ groups (-1.97 eV for BuDA, compared with -1.96 eV for MA on the surface of 3D perovskite). The long molecules bind very well to two perovskite layers and form Ruddlesden-Popper quasi-2D perovskite. However, the shorter molecule (butylammonium) binds to the two weaker perovskite layers, due to the less attractive van der Waals interactions between the -CH₂- chains. The weakest case, namely BuDA, is not a very good candidate to form the Dion Jacobson (DJ) perovskite structure. Details about these calculations are given in the supporting information.

The experiment for BuDA did not reveal any A cation exchange. We noted that the N-N distance between two ammonium groups in BuDA (6.32 Å) approaches the lattice vector of MAPbBr₃ (5.8-5.9 Å). Therefore, this barrier molecule meets two obstacles

when trying to enter the 3D crystal with MA vacancies, namely, two NH_3^+ groups are stacked between two subsequent PbBr_2 planes. Thus, further penetration into the crystal is impossible. Finally, we concluded that after the formation of the outermost quasi-2D perovskite layer, the barrier molecules still penetrate deeper into the 3D crystal phase until no more MA vacancies are available.

To assess the stability of the SCs after the dimensional transition, two experiments were done. Four SCs treated with different barrier molecules were analyzed by absorbance and XRD after six months after the transition was completed. The absorbance of each SC was measured and compared to that of a 3D SC (Figure S14). The onset of all single crystals protected by the 2D perovskite on their surface was stable after six months. (The slight shift observed in the SC absorbance can be attributed to variations in the SC thickness, as was explained previously). Moreover, XRD of the same crystals after exfoliation of the 2D perovskite from their surface was measured as can be seen in Figure S15. MAPbBr_3 peaks can be observed in these XRD measurements, which provide an additional proof for their stability.

Conclusions

Here, we investigated and tracked in detail the transition process from 3D MAPbBr_3 single-crystal perovskite to 2D perovskite. Three monoammonium barrier molecules and one di-ammonium barrier molecule were studied. Using Q-NMR and penetration depth (PD) measurements, we quantitatively monitored the transition dimensionality over time. It was found that the short aliphatic chain barrier molecules penetrate deeper into the SC than the long aliphatic chain barrier molecules; however, it takes more time for this to occur. CL and absorbance studies show that 2D perovskite, which formed on the SC surface, has a different dimensionality (i.e., mixed n values) and is not necessarily just $n=1$. DFT simulations for the transition process support the experimental results. Apparently, the MA vacancies initiate the penetration process, which depends on the concentration of the barrier molecules. The DJ 2D perovskite formed with the di-ammonium barrier molecule is much thinner than the RP 2D perovskites formed by the mono-ammonium barriers, due to the strong interactions between the NH_3 group and the PbBr_2 crystal planes that impede the whole process. Studies of dimensionality transition in SCs can serve as good models to better understand the kinetics and thermodynamics of 3D and 2D perovskites.

Experimental Section

Materials

PbBr₂ 98%, MABr 99.99% anhydros, 1,4-diaminobutane 99% nitrogen flashed, Hexylamine 99%, Octylamine 99%, Butylamine 99%, Ethanol absolute 98%, DMF 99.8% extra dry over a molecular sieve, DMSO 99.7% extra dry over a molecular sieve, isopropanol 99.5% anhydrous, isopropanol-d8 99.5%D, Ethyl ether extra pure.

Barrier molecule synthesis

Into a 100ml flask, a 5ml ethanol absolute and 5 ml of C_nNH₂ or 1,4-diaminobutane were added and stirred for 10 minutes. When the stirring was over, hydrobromic acid was slowly added dropwise into the solution. The two first levels of the synthesis were done in an ice bath. After the dripping was over, the solution kept stirring for 30 minutes inside an ice bath and then, more 90 minutes at room temperature. The solvent evaporation was done by using a rotatory evaporator at 60°C. The product was washed 3 times in ethyl-ether for 14 hours and then, filtered, and dried under vacuum.

MAPbBr₃ SCs growth

MAPbBr₃ SCs were grown through an anti-solvent vapor assisted crystallization. In an inert atmosphere glovebox, a 5ml perovskite solution was prepared. Into 18ml vial were added: 1.8350g PbBr₂, 0.5600g MABr, 0.8ml DMSO, and 4.2ml DMF. The solution was heated (70°C) for 2 hours. The vial with the solution was placed in an 100ml vial containing 40ml ethanol-absolute. MAPbBr₃ SCs appeared after 3 days and left growing for more than 10 days.

Transition dimensionality reaction

After filtering the MAPbBr₃ SCs, they were dipped inside different barrier molecules solutions (0.2M). The monoammonium barriers solutions contained the barrier salt and 1ml of dry isopropanol. The diammonium barrier solution contained the barrier salt and 1 ml mixture of dry methanol and formamide (95% and 5%).

Absorbance measurements

Absorbance spectrum were measured by using Cary5000 spectrophotometer with an integrated sphere (IS) holder FRA 2500 of Agilent. First, a microscope glass was cut to 1cm by 1.5cm size. Double-sided dap tape was put on the glass. The glass was attached to the IS, and the SC was attached to the glass.

CL measurements

CL pictures and spectrums were taken by using analytical high-resolution SEM Apreo. The spectrums were measured using Delmic SPARC CL system.

Scanning electron microscopy and PD

SEM images were taken by using an extra high-resolution SEM Magellan 400L (FEI). The voltage was 5 KV and the current was 13 μ A.

Quantitative NMR measurements

Inside an NMR test tube, a barrier solution was prepared. The test tube was taken for first measurement so-called time 0. After the first measurement, a SC was added into the test tube and then, was sealed with parafilm. The barrier integration is used as a standard for the concentration calculation from the integration. The test tube with the SC was measured every 5 days to see the change in the spectrum and integration (see the Q-NMR spectrums in fig. S4-6). The used magnet was Bruker 500 MHz.

Calculation details

We performed the DFT calculations for various geometric conformations in order to characterize the processes of the A cation exchange. We started with some predefined atomic structures and optimized both the atomic positions and the lattice vectors. We used the Quantum ESPRESSO code⁴⁹, that models the atomic cores with the pseudopotentials and the basis set contains the plane waves. The Perdew-Burke-Ernzerhof exchange-correlation functional was chosen. The ultrasoft pseudopotentials were used with the energy cutoffs of 35 Ry for the plane waves and 350 Ry for the density. The Monkhorst and Pack uniform grid for the Brillouin zone sampling was used, with the accuracy level of 8 k-points along each reciprocal-space vector equivalent to the lattice vector of about 6 Å. The geometries were optimized with the Broyden-Fletcher-Goldfarb-Shanno algorithm, with the criteria for energy and force set to 1.0E-04 Ry and 1.0E-03 Ry/Bohr, respectively.

Acknowledgment

The authors would like to thank the Israel Energy ministry of Science and the AFRL for their financial support.

References

- [1] G. Pacchioni, Nat Rev Mater 6 (2021).

- [2] Y. Liu, W. Yang, S. Xiao, N. Zhang, Y. Fan, G. Qu, Q. Song, *ACS Nano* 13 (2019).
- [3] A. Kostopoulou, K. Brintakis, N.K. Nasikas, E. Stratakis, *Nanophotonics* 8 (2019).
- [4] A. Efrati, S. Aharon, M. Wierzbowska, L. Etgar, *EcoMat* 2 (2020).
- [5] U.G. Jong, C.J. Yu, J.S. Ri, N.H. Kim, G.C. Ri, *Phys Rev B* 94 (2016).
- [6] D. Yu, B. Cai, F. Cao, X. Li, X. Liu, Y. Zhu, J. Ji, Y. Gu, H. Zeng, *Adv Mater Interfaces* 4 (2017).
- [7] S. Rahmany, L. Etgar, *Mater Adv* 2 (2021).
- [8] Y. Cho, A.M. Soufiani, J.S. Yun, J. Kim, D.S. Lee, J. Seidel, X. Deng, M.A. Green, S. Huang, A.W.Y. Ho-Baillie, *Adv Energy Mater* 8 (2018).
- [9] N.T. Shewmon, H. Yu, I. Constantinou, E. Klump, F. So, *ACS Appl Mater Interfaces* 8 (2016).
- [10] Y. Zhang, D. Lu, M. Gao, M. Lai, J. Lin, T. Lei, Z. Lin, L.N. Quan, P. Yang, *Proc Natl Acad Sci U S A* 116 (2019).
- [11] B. El Cohen, Y. Li, Q. Meng, L. Etgar, *Nano Lett* 19 (2019).
- [12] P. Li, C. Liang, X.L. Liu, F. Li, Y. Zhang, X.T. Liu, H. Gu, X. Hu, G. Xing, X. Tao, Y. Song, *Advanced Materials* 31 (2019).
- [13] C. Ma, C. Leng, Y. Ji, X. Wei, K. Sun, L. Tang, J. Yang, W. Luo, C. Li, Y. Deng, S. Feng, J. Shen, S. Lu, C. Du, H. Shi, *Nanoscale* 8 (2016).
- [14] T.M. Koh, V. Shanmugam, X. Guo, S.S. Lim, O. Filonik, E.M. Herzig, P. Müller-Buschbaum, V. Swamy, S.T. Chien, S.G. Mhaisalkar, N. Mathews, *J Mater Chem A Mater* 6 (2018).
- [15] A. Krishna, S. Gottis, M.K. Nazeeruddin, F. Sauvage, *Adv Funct Mater* 29 (2019).
- [16] E.T. McClure, A.P. McCormick, P.M. Woodward, *Inorg Chem* 59 (2020) 6010–6017.
- [17] M. Rahil, R.M. Ansari, C. Prakash, S.S. Islam, A. Dixit, S. Ahmad, *Sci Rep* 12 (2022) 2176.
- [18] X. Li, J. Hoffman, W. Ke, M. Chen, H. Tsai, W. Nie, A.D. Mohite, M. Kepenekian, C. Katan, J. Even, M.R. Wasielewski, C.C. Stoumpos, M.G. Kanatzidis, *J Am Chem Soc* 140 (2018) 12226–12238.
- [19] C. Ma, S. Wang, L. Gao, Z. Xu, X. Song, T. Yang, H. Li, X. Liu, S. (Frank) Liu, K. Zhao, *Adv Opt Mater* 11 (2023).
- [20] Z. Liu, K. Meng, X. Wang, Z. Qiao, Q. Xu, S. Li, L. Cheng, Z. Li, G. Chen, *Nano Lett* 20 (2020) 1296–1304.
- [21] G. Wu, R. Liang, M. Ge, G. Sun, Y. Zhang, G. Xing, *Advanced Materials* 34 (2022).

- [22] P. Giannozzi, S. Baroni, N. Bonini, M. Calandra, R. Car, C. Cavazzoni, D. Ceresoli, G.L. Chiarotti, M. Cococcioni, I. Dabo, A. Dal Corso, S. De Gironcoli, S. Fabris, G. Fratesi, R. Gebauer, U. Gerstmann, C. Gougoussis, A. Kokalj, M. Lazzeri, L. Martin-Samos, N. Marzari, F. Mauri, R. Mazzarello, S. Paolini, A. Pasquarello, L. Paulatto, C. Sbraccia, S. Scandolo, G. Sclauzero, A.P. Seitsonen, A. Smogunov, P. Umari, R.M. Wentzcovitch, *Journal of Physics Condensed Matter* 21 (2009).
- [23] H. Diab, C. Arnold, F. Lédée, G. Trippé-Allard, G. Delport, C. Vilar, F. Bretenaker, J. Barjon, J.-S. Lauret, E. Deleporte, D. Garrot, *J Phys Chem Lett* 8 (2017) 2977–2983.
- [24] D. Meggiolaro, E. Mosconi, F. De Angelis, *ACS Energy Lett* 4 (2019).
- [25] G. Volonakis, F. Giustino, *Appl Phys Lett* 112 (2018).
- [26] S. So, T. Badloe, J. Noh, J. Rho, J. Bravo-Abad, *Nanophotonics* 9 (2020).
- [27] L. Etgar, *Energy Environ Sci* 11 (2018).
- [28] Y. Kobori, K. Miyazaki, T. Tachikawa, Y. Ogomi, S. Hayase, *ECS Meeting Abstracts MA2017-01* (2017).
- [29] P. Guo, Q. Ye, C. Liu, F. Cao, X. Yang, L. Ye, W. Zhao, H. Wang, L. Li, H. Wang, *Adv Funct Mater* 30 (2020).
- [30] Y. Fang, H. Wei, Q. Dong, J. Huang, *Nat Commun* 8 (2017).
- [31] J. Ding, Q. Yan, *Sci China Mater* 60 (2017).
- [32] M.I. Dar, G. Jacopin, M. Hezam, N. Arora, S.M. Zakeeruddin, B. Deveaud, M.K. Nazeeruddin, M. Grätzel, *ACS Photonics* 3 (2016).
- [33] T. Sheikh, A. Shinde, S. Mahamuni, A. Nag, *ACS Energy Lett* 3 (2018).
- [34] Z. Tan, Y. Wu, H. Hong, J. Yin, J. Zhang, L. Lin, M. Wang, X. Sun, L. Sun, Y. Huang, K. Liu, Z. Liu, H. Peng, *J Am Chem Soc* 138 (2016).
- [35] L. Dou, A.B. Wong, Y. Yu, M. Lai, N. Kornienko, S.W. Eaton, A. Fu, C.G. Bischak, J. Ma, T. Ding, N.S. Ginsberg, L.W. Wang, A.P. Alivisatos, P. Yang, *Science* (1979) 349 (2015).
- [36] H. Tian, L. Zhao, X. Wang, Y.W. Yeh, N. Yao, B.P. Rand, T.L. Ren, *ACS Nano* 11 (2017).
- [37] Y. Liu, H. Ye, Y. Zhang, K. Zhao, Z. Yang, Y. Yuan, H. Wu, G. Zhao, Z. Yang, J. Tang, Z. Xu, S. (Frank) Liu, *Matter* 1 (2019).
- [38] Y. Xu, Y. Li, Q. Wang, H. Chen, Y. Lei, X. Feng, Z. Ci, Z. Jin, *Mater Chem Front* (2022).
- [39] M. Konstantakou, D. Perganti, P. Falaras, T. Stergiopoulos, *Crystals (Basel)* 7 (2017).
- [40] L.K. Ono, S. Liu, Y. Qi, *Angewandte Chemie - International Edition* 59 (2020).

- [41] D. Kim, J.H. Yun, M. Lyu, J. Kim, S. Lim, J.S. Yun, L. Wang, J. Seidel, *Journal of Physical Chemistry C* 123 (2019).
- [42] S. Shrestha, X. Li, H. Tsai, C.H. Hou, H.H. Huang, D. Ghosh, J.J. Shyue, L. Wang, S. Tretiak, X. Ma, W. Nie, *Chem* 8 (2022).
- [43] R. Gupta, T.B. Korukonda, S.K. Gupta, B.P. Dhamaniya, P. Chhillar, R. Datt, P. Vashishtha, G. Gupta, V. Gupta, R. Srivastava, S. Pathak, *J Cryst Growth* 537 (2020).
- [44] Z. Chen, Q. Dong, Y. Liu, C. Bao, Y. Fang, Y. Lin, S. Tang, Q. Wang, X. Xiao, Y. Bai, Y. Deng, J. Huang, *Nat Commun* 8 (2017).
- [45] X.F. He, *Phys Rev B* 43 (1991).
- [46] B. Saparov, D.B. Mitzi, *Chem Rev* 116 (2016).
- [47] S. Govinda, B.P. Kore, M. Bokdam, P. Mahale, A. Kumar, S. Pal, B. Bhattacharyya, J. Lahnsteiner, G. Kresse, C. Franchini, A. Pandey, D.D. Sarma, *Journal of Physical Chemistry Letters* 8 (2017).
- [48] M.I. Saidaminov, A.L. Abdelhady, B. Murali, E. Alarousu, V.M. Burlakov, W. Peng, I. Dursun, L. Wang, Y. He, G. MacUlan, A. Goriely, T. Wu, O.F. Mohammed, O.M. Bakr, *Nat Commun* 6 (2015).
- [49] M.E. Kamminga, H.H. Fang, M.R. Filip, F. Giustino, J. Baas, G.R. Blake, M.A. Loi, T.T.M. Palstra, *Chemistry of Materials* 28 (2016).
- [50] W.J. Yin, J.H. Yang, J. Kang, Y. Yan, S.H. Wei, *J Mater Chem A Mater* 3 (2015).
- [51] A. Thote, I. Jeon, J.W. Lee, S. Seo, H.S. Lin, Y. Yang, H. Daiguji, S. Maruyama, Y. Matsuo, *ACS Appl Energy Mater* 2 (2019).
- [52] Z. Zhang, L. Ren, H. Yan, S. Guo, S. Wang, M. Wang, K. Jin, *Journal of Physical Chemistry C* 121 (2017).
- [53] Y. Gupta, S. Rathore, A. Singh, A. Kumar, *J Alloys Compd* 901 (2022).
- [54] A.S. Bhalla, R. Guo, R. Roy, *Materials Research Innovations* 4 (2000) 3–26.